CRYSTAL GROWTH & DESIGN
2004
VOL. 4, NO. 6
1351−1357

Screw Dislocations on Polycenes: A Requirement for Crystallization

H. M. Cuppen, W. S. Graswinckel, and H. Meekes*

Solid State Chemistry, University of Nijmegen, Toernooiveld 1, 6525 ED, Nijmegen, The Netherlands

Received July 16, 2004

ABSTRACT: The morphology and growth behavior of naphthalene, anthracene, and tetracene is studied both experimentally and by computer simulations. We will show that the attachment energy morphology prediction for all compounds gives approximately the correct habit, but that this is merely coincidental. Our Monte Carlo simulations and vapor growth experiments show that the thickness growth of the crystals perpendicular to the {001} faces is due to spirals on that face. If these screw dislocations were not present, the basal faces would not grow and no crystal would be formed at moderate driving force. At very high driving forces, very thin plates without screw dislocations were observed, with a morphology that is in agreement with the results of our Monte Carlo simulations.

1 Introduction

Many studies have been devoted to a better understanding and control of the external shape or morphology of crystals.[1−9] Most of these studies are from a later date than the famous BCF theory on spiral growth by Burton, Cabrera, and Frank.[10] Nevertheless, to our knowledge, all ignore the relevance of the spiral growth mechanism in their approach. Frank was the first to realize that a screw dislocation can provide an inexhaustible source of steps. These steps allow crystal faces to grow at small driving forces where the nucleation barrier for 2D nucleation is too high to get appreciable growth.[11] The present paper discusses the morphology and growth rate of the most important crystal faces of three compounds: naphthalene, anthracene, and tetracene. We will show that the attachment energy morphology prediction[12] for all compounds gives approximately the correct habit, but that this is merely coincidental. Our Monte Carlo simulations and vapor growth experiments show that the thickness of the crystals in the (001) direction is due to spirals on that face. Without dislocations present on this surface no crystals will be formed at moderate driving forces. The three compounds have homologous molecular structures and similar crystal structures. Two of the three compounds, naphthalene and anthracene, crystallize in spacegroup $P2_1/a$. Tetracene has spacegroup $P\bar{1}$, but the structure has a symmetry close to $P2_1/a$.

Table 1 gives the experimentally determined cell parameters as obtained from the Cambridge Structural Database (CSD) as well as the sublimation enthalpies.[13] Since the three compounds have similar molecular and crystallographic structures, they also have similar morphologies. The morphologies of naphthalene and anthracene are already discussed in detail by Grimbergen et al.[14] Docherty and Roberts[15] compared the morphology of anthracene with those of biphenyl and β-succinic acid, which grow in similar crystal structures but are energetically very different compounds. Here we extend the analysis of Grimbergen et al. with the morphology of tetracene. Moreover, Monte Carlo simulations are performed for all three compounds and compared with surface studies of anthracene and tetracene. The experimental data presented here are all obtained from crystals grown from the vapor phase. In this way, both the experiments and simulations are not influenced by any solvent.

Table 1. Cell Parameters and Sublimation Enthalpies of the Three Structures[a]

	naphthalene		anthracene		tetracene	
	exp	min	exp	min	exp	min
a (Å)	8.14	8.13	8.55	8.35	7.90	7.85
b (Å)	5.95	6.05	6.02	6.17	6.03	6.10
c (Å)	8.66	8.74	11.17	11.14	13.53	13.52
α (°)	90.0	90.0	90.0	90.0	100.3	99.5
β (°)	124.1	123.5	126.6	124.4	113.2	113.1
γ (°)	90.0	90.0	90.0	90.0	86.3	86.2
ΔH°_{sub} (kcal/mol)	19 ± 1		23 ± 2		30 ± 5	
$E_{lattice}$ (kcal/mol)		−19.41		−26.1		−34.3

[a] The left value is the experimental value; the right value is obtained after minimization.

2 Experimental Morphologies

Crystals of anthracene and tetracene were grown from the vapor in a specially designed in-situ cell,[16,17] which allows the temperature of the evaporating source material (T_1) and the substrate (T_2) to be controlled independently. An equilibrium vapor pressure is maintained with respect to the source material at all times; this implies that the driving force at the substrate depends solely on the chosen temperatures T_1 and T_2. A low background pressure (10^{-3} mbar) was used.

The crystals were nucleated at a large temperature difference, i.e., high driving force, after which it was lowered to obtain crystals of high quality. Glass was used as substrate. Crystals of tetracene were typically nucleated at 100 °C/93 °C (T_1/T_2) and grown at 100 °C/97 °C. Typical growth temperatures for anthracene were 30 °C/29.9 °C.

Crystals were analyzed using optical microscopy and atomic force microscopy (AFM). AFM measurements on anthracene were found to be difficult due to rapid evaporation.

Naphthalene, anthracene, and tetracene all have hexagonal, platelike morphologies. Figure 1a shows the morphology of anthracene; Figure 1b is that of tetracene. For the morphology of naphthalene grown from the vapor we refer to Grimbergen et al.[14] Figure 1,

10.1021/cg049756q CCC: $27.50
Published on Web 10/08/2004

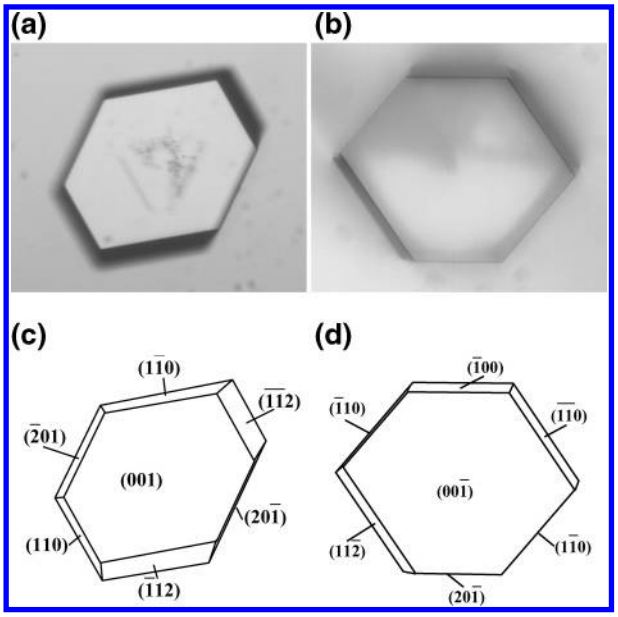

Figure 1. Experimental morphologies of (a) anthracene grown at 30 °C/29.9 °C (T_1/T_2) and (b) tetracene grown at 100 °C/97 °C. Image (b) is composed from two images focused at the top and the middle of the crystal. Panel (c) gives a schematic representation of (a) and (d) of (b).

panels c and d show a schematic representation of the morphologies of anthracene and tetracene, respectively. The large basal face is in both cases the {001} face. Since the crystals are too small to index on a goniometer, the side faces were determined by comparing two images: one focused at the top of the crystal and one at the middle. The distances and angles between the points which are in focus determine the index of the faces. Here we indicated the faces with Miller indices with the smallest possible numbers and do not account for the crystallographic selection rules. The anthracene crystal shown in Figure 1a has side faces: {20$\bar{1}$}, {11$\bar{2}$}, and {110}. At higher driving forces also anthracene crystals with {20$\bar{1}$}, {11$\bar{1}$}, {110}, and {10$\bar{1}$} faces were observed. The tetracene crystals have side faces {100}, {20$\bar{1}$}, {11$\bar{2}$}, {110}, and {1$\bar{1}$0}. At higher driving forces also tetracene crystals with {20$\bar{1}$}, {11$\bar{1}$}, {1$\bar{1}\bar{1}$}, {110}, {1$\bar{1}$0}, and {10$\bar{1}$} faces were observed.

3 Connected Net Analysis

The experimentally observed morphologies are compared with morphologies obtained from the attachment energy method and Monte Carlo simulations. To come to these morphologies, first the crystal graph is determined. A crystal graph is a model representation of the crystal structure in which spheres stand for the growth units and lines connecting the spheres stand for the intermolecular interactions. The first step in constructing a crystal graph is the optimization of the crystal structure with respect to energy using molecular mechanics. We used the Cerius[2] program for this purpose. The Dreiding force field[18] in combination with ESP derived point charges was used. Table 1 gives the cell parameters after minimization, and Figure 2a shows the corresponding crystal structure of anthracene. The lattice energies in the last row are quite close to the experimental sublimation enthalpies. This is an indication of the quality of the force field for this type of molecule.

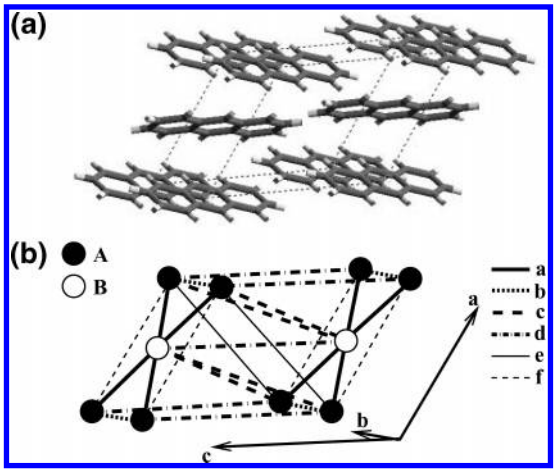

Figure 2. (a) The crystal structure of anthracene. (b) The general crystal graph for all structures with the bonds defined in Table 2.

Table 2. The Crystal Graphs[a]

				naphthalene		anthracene		tetracene	
label	GU1	GU2	[*uvw*]	length	E_{bond}	length	E_{bond}	length	E_{bond}
a	A	B	[000]	5.07	−4.53	5.19	−6.74	5.13	−9.31
a′	A	B	[010]					4.81	−9.82
b	A	A	[010]	6.05	−3.27	6.17	−4.48	6.10	−6.90
b′	B	B	[010]					6.10	−6.94
c	A	B	[001]	7.93	−1.54	9.92	−1.69	12.41	−1.42
c′	A	B	[01$\bar{1}$]					13.34	−1.09
d	A	A	[001]	8.74	−1.06	11.14	−1.02	13.52	−1.16
d′	B	B	[001]					13.52	−0.89
e	A	A	[101]	8.00	−0.59	9.42	−0.67		
f	A	A	[100]					7.85	−0.72
f′	B	B	[100]					7.85	−0.75

[a] The first growth unit (GU1) is always in unit cell [000]. Energies are given in kcal/mol and lengths are in Å. The *x* and *x′* bonds are symmetry-related for naphthalene and anthracene.

The next step is to determine the intermolecular interactions of all growth units within a certain range. The interactions stronger than $\approx 1kT$ (0.6 kcal/mol for 310 K) are included in the crystal graph. For all compounds, this corresponds to the five strongest bonds. Table 2 gives these bonds and their corresponding energies and lengths. This table should be read as follows. Bond *b* connects growth unit A in cell [000] with growth unit A which is in cell [010] as is shown in Figure 2b.

For naphthalene and anthracene, the spacegroup symmetry results in sets of four symmetry-related bonds. For tetracene, the lower symmetry breaks these sets in two sets of two symmetry-related bonds. These two sets are labeled *x* and *x′* in Table 2. The table shows that the bonds of these sets are comparable in bond strength, indicating the small symmetry breaking for tetracene. Tetracene has almost the same set of bonds as anthracene and naphthalene. It only misses bonds *e*; instead the bonds *f* and *f′* are present.

Next, all connected nets[14] of the three structures are determined by using the program FACELIFT[19] with the crystal graph as input. Table 3 shows the attachment energies of the strongest connected net for all flat faces for the three structures. Since the crystal graphs of naphthalene and anthracene contain the same set of bonds, they have the same connected faces. Tetracene has a very similar set of connected faces since it also has a very similar graph. Not all faces that are symmetry-related for the $P2_1/a$ crystal graphs are symmetr-related for tetracene; this is due to its lower space group

Table 3. All Connected Faces[a]

	naphthalene			anthracene			tetracene		
	E_{hkl}^{att}	MI_{hkl}^{att}	MI_{hkl}^{MC}	E_{hkl}^{att}	MI_{hkl}^{att}	MI_{hkl}^{MC}	E_{hkl}^{att}	MI_{hkl}^{att}	MI_{hkl}^{MC}
{001}	−9.47	1	1	−10.16	1	1	−7.07	1	1
{11$\bar{1}$}	−20.80	3	3	−27.86	3	3	−38.16	7	4
{1$\bar{1}$1}							−39.84	9	5
{011}	−23.53	5		−30.90	5		−38.95	10	
{01$\bar{1}$}							−38.62	8	
{110}	−19.87	2	2	−27.17	2	2	−36.76	5	2
{1$\bar{1}$0}							−37.13	6	3
{20$\bar{1}$}	−21.43	4	4	−30.35	4	4	−41.78	11	4
{10$\bar{1}$}	−26.40	6		−35.77	7		−25.16	3	8
{100}	−25.47	7		−35.08	6		−23.11	2	7
{21$\bar{1}$}	−26.52	8		−35.95	8		−48.82	13	
{211}							−48.30	12	
{010}	−30.82	9		−42.69	9		−36.48	4	
{021}							−56.99	15	
{02$\bar{1}$}							−56.33	14	

[a] The left column gives the attachment energy in kcal/mol and the second and third columns give the order in morphological importance on the basis of the attachment energy method and the Monte Carlo simulations, respectively.

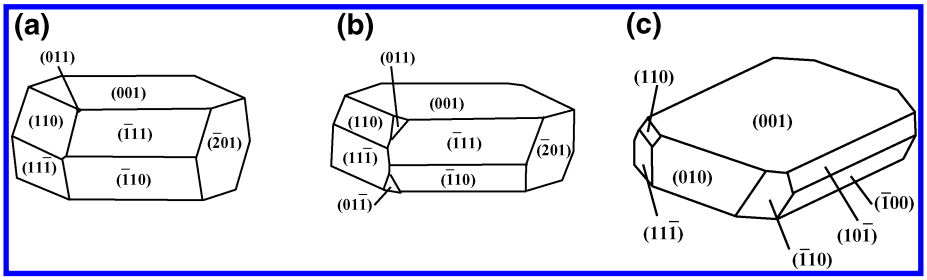

Figure 3. (a−c) The attachment energy morphologies of the three structures obtained from the connected net analysis and eq 1.

symmetry leading to different attachment energies for these faces.

Assuming that the growth rate of a face is proportional to its attachment energy

$$R_{hkl} \propto E_{hkl}^{att} \quad (1)$$

a morphology can be constructed using a Chernov-Wulff construction. Figure 3 gives the attachment energy morphologies of the three structures using the information in Table 3. For naphthalene and anthracene, the morphologies are very similar, except for the {011} faces which are larger for anthracene. Tetracene has at first sight a morphology similar to the other two, but it possesses different side faces.

The attachment energy morphologies shown for anthracene and naphthalene are very close to the experimentally observed morphologies shown in Figure 1 and in ref 14 except for the {11$\bar{2}$} faces which are only occasionally observed. The attachment energy morphology of tetracene contains faces {010}, {11$\bar{1}$}, and {10$\bar{1}$}, which are not present in the experimentally observed morphology and is lacking the observed {20$\bar{1}$} and {11$\bar{2}$} faces. The {11$\bar{2}$} faces are not connected for this crystal graph.

4 Monte Carlo Simulations: Method and Results

The Monte Carlo simulation program MONTY is able to simulate the growth of any face of any crystal structure at any temperature and driving force. Both the birth-and-spread mechanism or a combination of spiral growth and birth-and-spread can be implemented. The program uses a crystal graph of the crystal structure as input. We refer to Boerrigter et al.[20] for more details on the program. The growth of all F-faces (Table 3) is simulated using MONTY at a temperature of 310 K and a broad range of driving forces.

For the attachment and detachment probabilities of the growth units the random rain scheme[21,22] was used. This can be achieved by setting the kinetic parameters λ_1 and λ_2 as introduced by Boerrigter et al. to zero. The random rain scheme gives a good description of the direct incorporation during vapor growth,[23] although surface diffusion, which is ignored here, might be important. All growth units enter the surface at confined sites as described by the crystal graph. During the simulations we measure the growth rate R.

Figure 4, panels a, b, and c show the growth rate as a function of the driving force for the connected faces of naphthalene, anthracene, and tetracene. The solid curves indicate the faces which are grown via the 2D nucleation mechanism without the presence of screw dislocations. All figures show separate growth rate curves for the slow growing faces and a bundle of curves for the fast growing faces. Table 3 indicates the order in growth rate for the slow growing faces.

For all compounds, the basal {001} faces grow much slower than the other faces. This would result in very thin plates as is shown in Figure 6, panels a, c, and e for naphthalene, anthracene, and tetracene, respectively. These thin plates are not in correspondence with the experimentally observed morphologies shown previously. One explanation for this discrepancy between experimental morphologies and our Monte Carlo results could be the presence of screw dislocations ending on the basal {001} face. The face would then grow via growth spirals resulting in a higher growth rate.

The dashed curves in Figure 4 represent the growth rates of the faces grown with the spiral mechanism. For anthracene, simulations with screw dislocations were performed for all faces. Comparison of Figure 4, panels

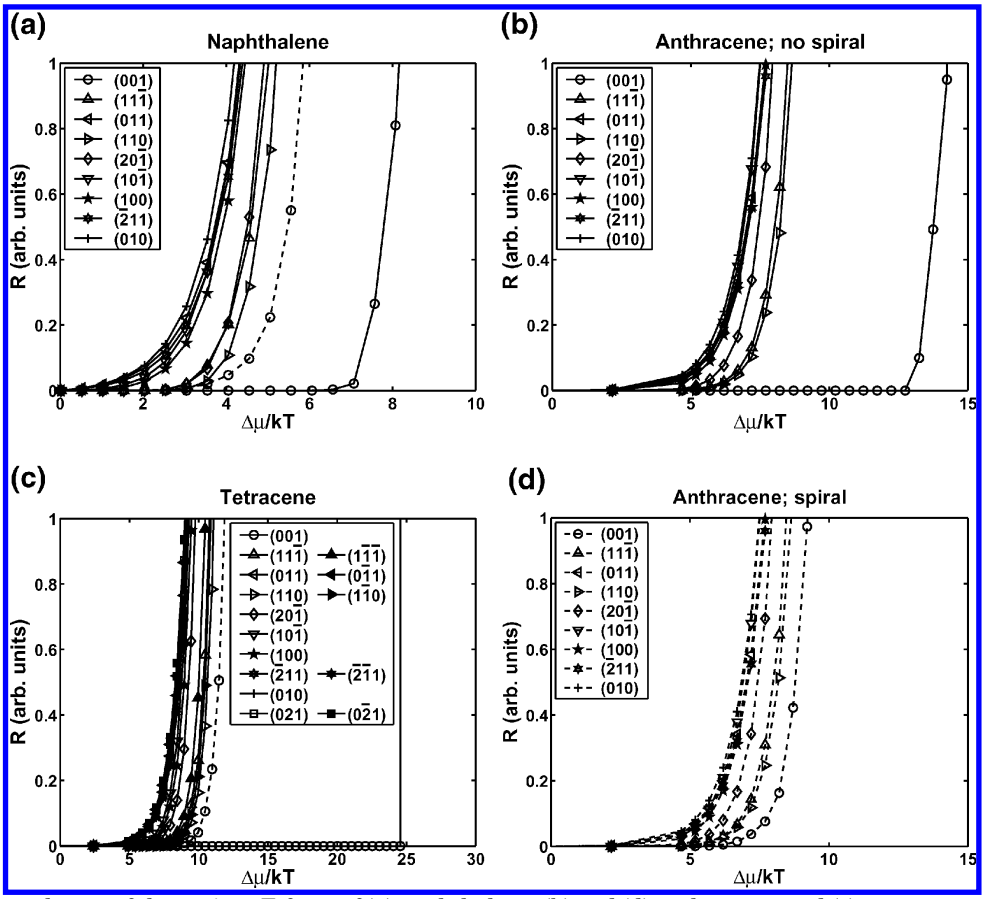

Figure 4. The growth rate of the various F-faces of (a) naphthalene, (b) and (d) anthracene, and (c) tetracene as a function of the driving force. The solid curves indicate the faces that are grown via the 2D nucleation mechanism without the presence of screw dislocations; the dashed curves with screw dislocations present.

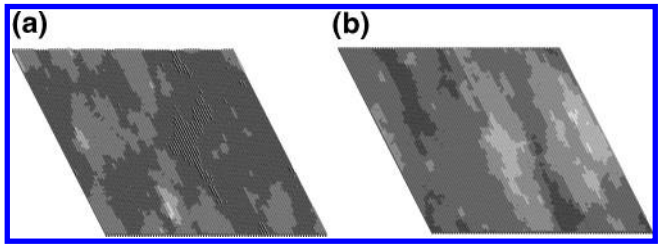

Figure 5. Two snapshots taken during Monte Carlo simulations of (110) surfaces for anthracene. Panel (a) shows a perfect surface; (b) a surface with one screw dislocation. Both surfaces are simulated at $T = 310$ K and with a driving force of $\Delta\mu = 6.7kT$.

b and d for anthracene shows that only the growth rate of the {001} faces is strongly affected by the presence of the screw dislocations. For the other faces 2D nucleation is already possible at low driving forces and the spiral growth mechanism is not needed to speed up the growth process. For the {001} face, the nucleation barrier is extremely high as compared to the other faces and the presence of growth spirals enhances growth dramatically. Figure 5 shows two snapshots taken during Monte Carlo simulations of the (110) surfaces. One is simulated in the presence of a screw dislocation and one without. The driving force is chosen such that growth rate is relatively low. The surfaces show many 2D nuclei, even at this low growth rate. On the surface with the screw dislocation no distinct spiral hillock has developed.

Since the anthracene crystal shows that the spiral growth mechanism is only important for the {001} face, only this face is simulated in the presence of screw dislocations for the naphthalene and tetracene structures. Also for these structures the effect of the screw dislocations on the {001} faces is tremendous judging from Figure 4a,c. Figure 6, panels b, d, and e show the corresponding morphologies. These morphologies have aspect ratios much closer to the experimental morphologies. The morphologies lack several orientations which are found experimentally. The order in morphological importance is however correctly predicted (Table 3), except for the {11$\bar{2}$} faces, which were not simulated as they are not connected on the basis of the present crystal graph. This is in contrast with the attachment energy morphology, which shows large {010}, {11$\bar{1}$}, and {10$\bar{1}$} faces, which are experimentally not observed, but misses the {20$\bar{1}$} faces, which are observed.

5 Proof for the Spiral Growth Mechanism

To check our hypothesis that the thicker morphologies are caused by the presence of screw dislocations, we examined the {001} surface of anthracene and tetracene for the presence of spiral hillocks by means of optical microscopy and AFM. For both anthracene and tetracene spiral hillocks were observed. We studied several anthracene and tetracene crystals. In all cases, the {001} faces are fully covered with spiral steps protruding from screw dislocations. Figure 7a shows a spiral hillock on the {001} surface of anthracene observed by AFM. Step heights of 8−9 Å are found for steps on the anthracene crystals, which is in agreement with the interplanar distance of anthracene, $d_{001} = 9.19$ Å. The

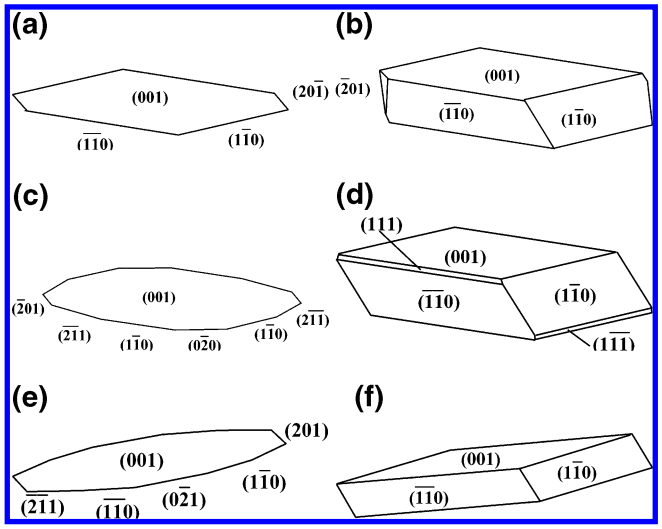

Figure 6. The morphologies obtained from Monte Carlo simulations as presented in Figure 4 without screw dislocations of (a) naphthalene at $\Delta\mu = 7.1kT$, (c) anthracene at $\Delta\mu = 13.2kT$, and (e) tetracene at $\Delta\mu = 25.1kT$. The right panels show morphologies with screw dislocations present on the basal {001} faces for (b) naphthalene at $\Delta\mu = 4.6kT$ and (f) tetracene at $\Delta\mu = 9.5kT$. Panel (d) shows the morphology of anthracene at $\Delta\mu = 8.7kT$ with screw dislocations on all faces.

spiral hillock on this face is strongly damaged by evaporation after removing the crystal from the cell. We will therefore in the remainder mainly focus on the ex situ AFM observations of tetracene crystals, which have a lower vapor pressure.

Figure 7b–d shows typical surfaces of basal faces of tetracene crystals. Figure 7b shows a double spiral, Figure 7c shows several screw dislocations, some with a Burgers vector larger than one lattice spacing, and Figure 7d shows a single spiral outcrop. This spiral was large enough to cover the whole surface. The step heights measured for the tetracene surfaces are approximately 10 Å, which is close to the interplanar distance of d_{001} = 12:30 Å. In both cases, anthracene and tetracene, the measured step height is within the accuracy of the AFM. The screw dislocation in Figure 7d is the only isolated screw dislocation. One should only consider the spiral arms which are far away from the outcrop of the screw dislocation, since the arms close to the outcrop are altered during the removal of the crystal from its growth environment. The spiral has four main sides and one smaller side in the right lower corner of the spiral. Note that the spiral has an anisotropy which differs from the observed shape of the basal face in the macroscopic morphology.

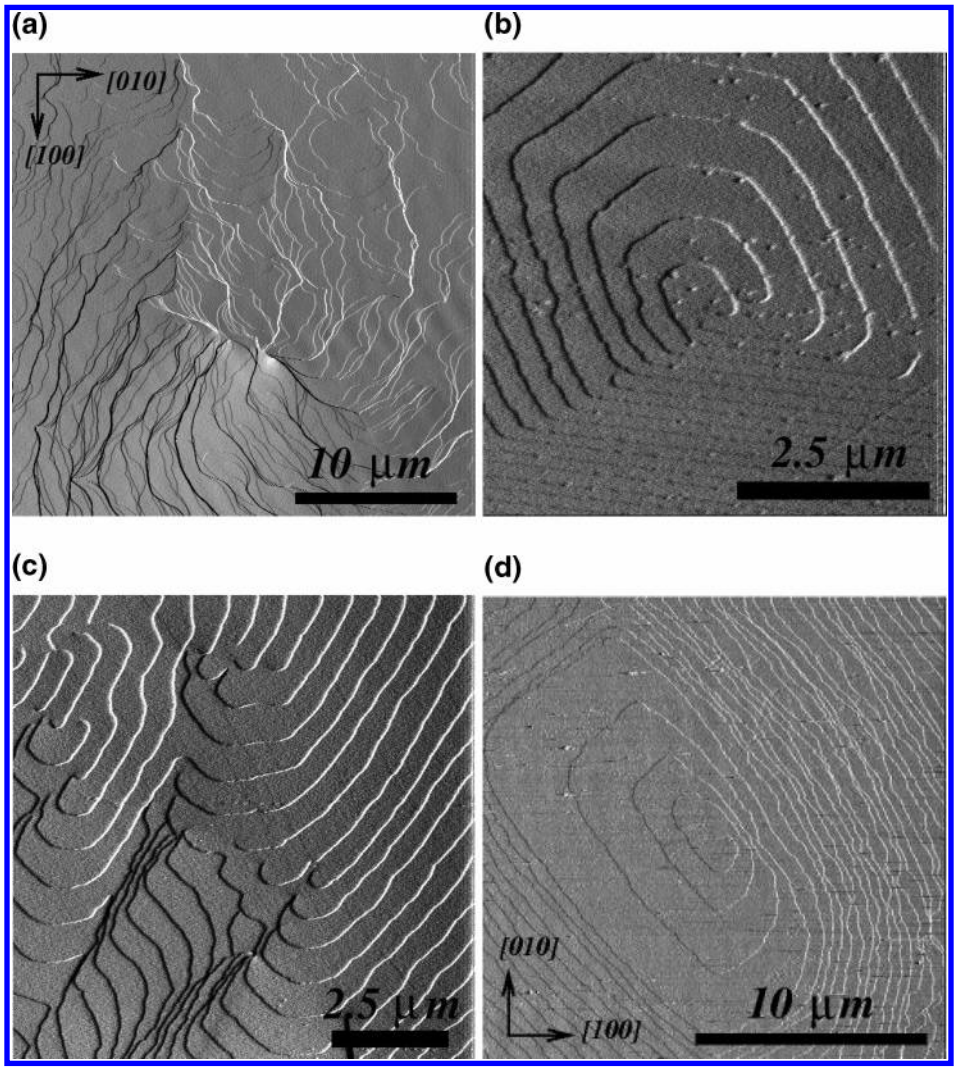

Figure 7. Spiral hillocks on the basal {001} face of (a) anthracene and (b–d) tetracene observed experimentally by means of atomic force microscopy.

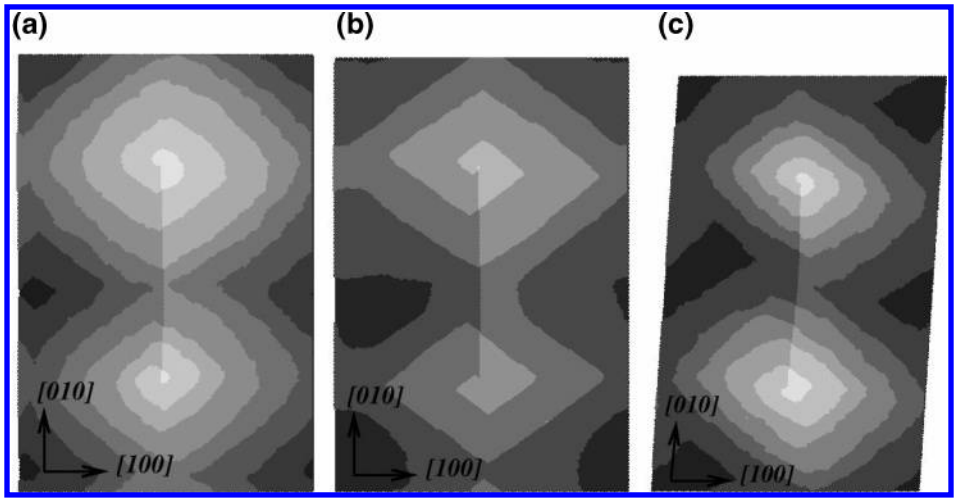

Figure 8. Spiral hillocks on the basal {001} face of (a) naphthalene at $\Delta\mu = 4.0kT$, (b) anthracene at $\Delta\mu = 6.7kT$, and (c) tetracene at $\Delta\mu = 12kT$ obtained by Monte Carlo simulations.

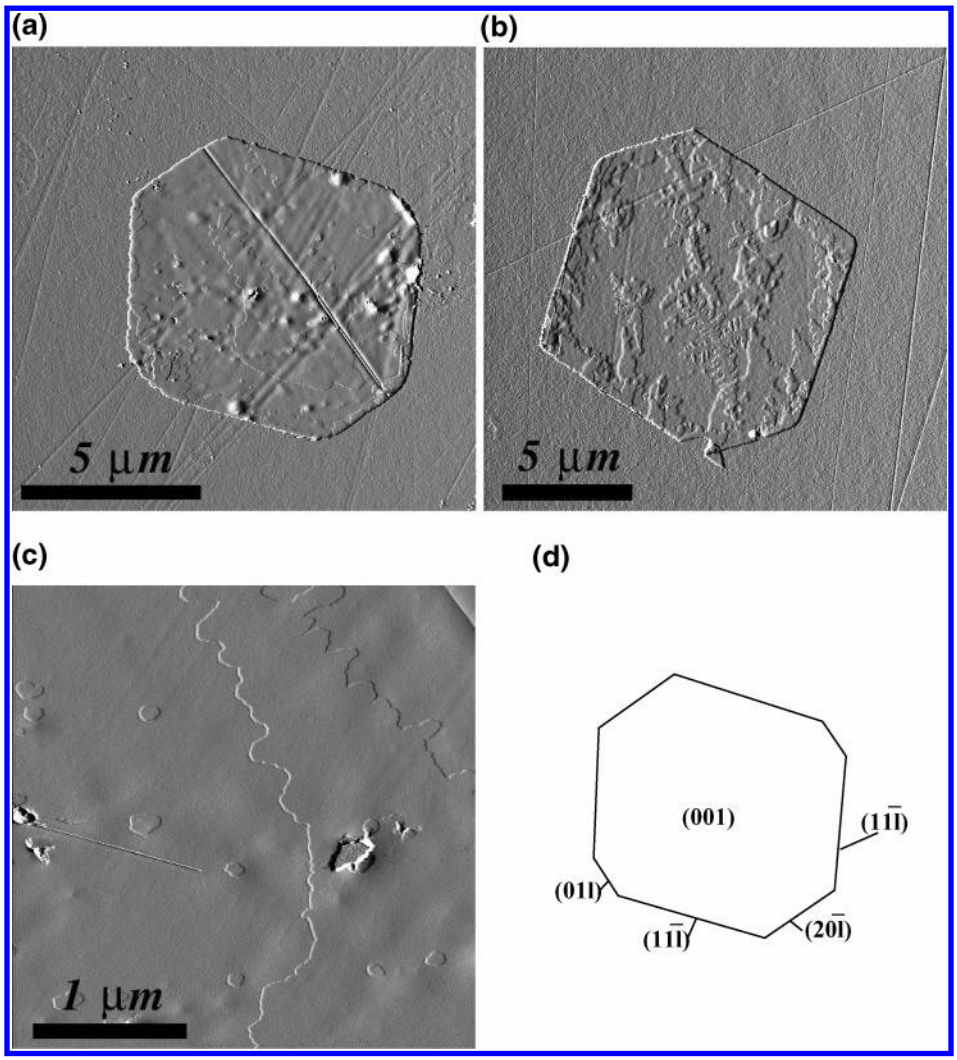

Figure 9. (a−c) AFM images of tetracene crystals grown at very high driving forces. Panels (a) and (b) show the whole crystal; (c) a detail of the surface; (d) gives a schematic representation of the morphology of these thin crystals.

Figure 8 shows three simulated spirals on the {001} face of naphthalene, anthracene, and tetracene, all consisting of two main sides. It appears that the simulated spirals, like the morphologies, are lacking certain directions. This might explain the limited quality of the predictions found for the side faces.

6 Crystals without Screw Dislocations

The crystals presented in the previous sections are all grown at relatively low driving forces. As Figure 4 shows the {001} faces without dislocations do not grow at low driving forces. This means that crystals with

defect-free {001} faces are not able to grow out to be large enough to be observed and only crystals with dislocations will appear. If the driving force is high enough for the {001} faces to grow without dislocations, also crystals with perfect {001} faces would be observed. These crystals would have morphologies as presented in Figure 6, panels a, c, and e. The side faces are, for these high driving force, kinetically rough and the morphology will therefore be rounded.

Very small crystals were grown at high driving forces by simply heating the bottom of a glass vial containing a small amount of tetracene to 200 °C. This produces a highly supersaturated vapor, in which homogeneous 3D nucleation of crystallites takes place. The small convecting crystallites were collected on a glass substrate and were examined by AFM. Figure 9a,b shows two of the thus formed crystallites. The crystallite in the left image has a thickness of approximately 15 unit cells; the crystal in the right image is of some 10 unit cells. The sharp patterns on the surfaces indicate the nuclei on the top side of the crystal; the less clear patterns are on the bottom side. Both crystallites only show 2D nucleation and do not possess spiral hillocks. This proves that crystals without screw dislocations have morphologies similar to Figure 6e. These crystals can however only be formed at very high driving forces. At low driving force, only crystals with screw dislocations can be formed.

7 Conclusions

The present paper shows that the crystals of naphthalene, anthracene, and tetracene which are grown under normal growth conditions always have screw dislocations on the basal {001} faces. If these screw dislocations are not present, the basal faces cannot grow and no crystal will be formed at moderate driving forces. We expect this observation to be generally true for comparably anisotropic crystal structures. Monte Carlo simulations of all important faces of anthracene in the presence of screw dislocations showed that the growth rate of all faces except the slow growing {001} faces are hardly affected as compared to the growth rate of defect-free faces. This means that the aspect ratio of the crystals is much smaller in the presence of screw dislocations. A similar situation was found for gibbsite (γ-$Al(OH)_3$) crystals[24,25] and paraffin crystals.[26]

The attachment energy morphology prediction method resulted in morphologies that are reasonably close to the observed morphologies. This method generally gives blocklike morphologies with a too low aspect ratio. This is because the attachment energies are the result of the sum of various interactions in the crystal graph, whereas in reality the step energies play an important role in determining the growth rate and they are often determined by the sums and differences of bond energies. This leads to much larger aspect ratios. The present paper shows that this larger aspect ratio is reduced again by the presence of screw dislocations.

Needle crystals also have a high anisotropy in step energies leading to their large aspect ratio in morphology. For needle crystals, it is however much more difficult to develop spirals that contribute to the growth of the slow growing side faces, since these faces are often too narrow for spirals to be able to rotate in the nucleation phase. Needle crystal can therefore often only be formed at driving forces high enough to support 2D nucleation on the side faces.[27]

To generalize the reasoning of the present study, crystals with small aspect ratios due to the presence of screw dislocations on the slow growing faces are more often observed than very thin, defect-free, platelets. The reason for this is that the latter can either not be formed at moderate driving forces or they are ignored or not observed among the more blocklike crystals.

Acknowledgment. The authors would like to thank B.M.A. van der Wolf and R. Algra for their vapor growth experiments and AFM measurements. H.M.C. would like to thank the Council for Chemical Sciences of The Netherlands Organisation for Scientific Research (CW-NWO) for financial support.

References

(1) Donnay, J. D. H.; Harker, D. *Am. Mineral.* **1937**, *22*, 446−467.
(2) Hartman, P.; Perdok, W. G. *Acta Crystallogr.* **1955**, *8*, 49.
(3) Hartman, P.; Perdok, W. G. *Acta Crystallogr.* **1955**, *8*, 521.
(4) Hartman, P.; Perdok, W. G. *Acta Crystallogr.* **1955**, *8*, 525.
(5) Follner, H. *Fortschr. Miner.* **1988**, *66*, 37−68.
(6) Docherty, R.; Clydesdale, G.; Roberts, K. J.; Bennema, P. *J. Phys. D* **1991**, *24*, 89−99.
(7) Clydesdale, G.; Roberts, K. J.; Docherty, R. *J. Cryst. Growth* **1996**, *166*, 78−83.
(8) Grimbergen, R. F. P.; Meekes, H.; Bennema, P.; Strom, C. S.; Vogels, L. J. P. *Acta Crystallogr. A* **1998**, *54*, 491−500.
(9) Gadewar, S. B.; Hofmann, H. M.; Doherty, M. F. *Cryst. Growth Des. 4* **2004**, 109−112.
(10) Burton, W. K.; Cabrera, N.; Frank, F. C. *Philos. Trans. R. Soc. London* **1951**, *243*, 299.
(11) Frank, F. C. *Discuss. Faraday Soc. 5* **1949**, *48*, 67.
(12) Hartman, P.; Bennema, P. *J. Cryst. Growth* **1980**, *49*, 145−156.
(13) Linstrom, P. J.; Mallard, W. G.; Eds.; National Institute of Standards and Technology: Gaithersburg MD, 20899 (http://webbook.nist.gov) 2003.
(14) Grimbergen, R. F. P.; Reedijk, M. F.; Meekes, H.; Bennema, P. *J. Phys. Chem. B* **1998**, *102*, 2646−2653.
(15) Docherty, R.; Roberts, K. J. *J. Cryst. Growth* **1988**, *88*, 159−168.
(16) Graswinckel, W. S.; van Enckevort, W. J. P., to be published.
(17) Noorduin, W.; Graswinckel, W. S.; van Enckevort, W. J. P., to be published.
(18) Mayo, S. L.; Olafson, B. D.; Goddard, W. A., III *J. Phys. Chem.* **1990**, *94*, 8897−8909.
(19) Boerrigter, S. X. M.; Grimbergen, R. F. P.; Meekes, H. 2001, FACELIFT-2.50, a program for connected net analysis; Department of Solid State Chemistry, University of Nijmegen, hugom@sci.kun.nl.
(20) Boerrigter, S. X. M.; Josten, G. P. H.; van de Streek, J.; Hollander, F. F. A.; Los, J.; Cuppen, H. M.; Bennema, P.; Meekes, H. *J. Phys. Chem. A* **2004**, *108*, 5894−5902.
(21) Gilmer, G. H.; Bennema, P. *J. Appl. Phys.* **1972**, *43*, 1347−1360.
(22) van der Eerden, J. P. Crystal Growth Mechanisms, In *Handbook of Crystal Growth*; Hurle, D. T. J., Ed.; Elsevier: Amsterdam, 1993; Vol. 1a, Chapter 5, p 307.
(23) Cuppen, H. M.; Meekes, H.; van Enckevort, W. J. P.; Bennema, P.; Vlieg, E. *Surf. Sci.* **2003**, *525*, 1−12.
(24) Sweegers, C.; Plomp, M.; de Coninck, H. C.; Meekes, H.; van Enckevort, W. J. P. *Appl. Surf. Sci.* **2002**, *187*, 218−234.
(25) Sweegers, C.; Boerrigter, S. X. M.; Grimbergen, R. F. P.; Meekes, H. *Phys. Chem. B* **2002**, *106*, 1004−1012.
(26) Plomp, M.; van Enckevort, W. J. P.; van Hoof, P. J. C. M.; van de Streek, C. J. *J. Cryst. Growth* **2003**, *249*, 600−613.
(27) Cuppen, H. M.; van Eerd, A. R. T.; Meekes, H. *Cryst. Growth Des.* **2004**, 4, 989−997.

CG049756Q